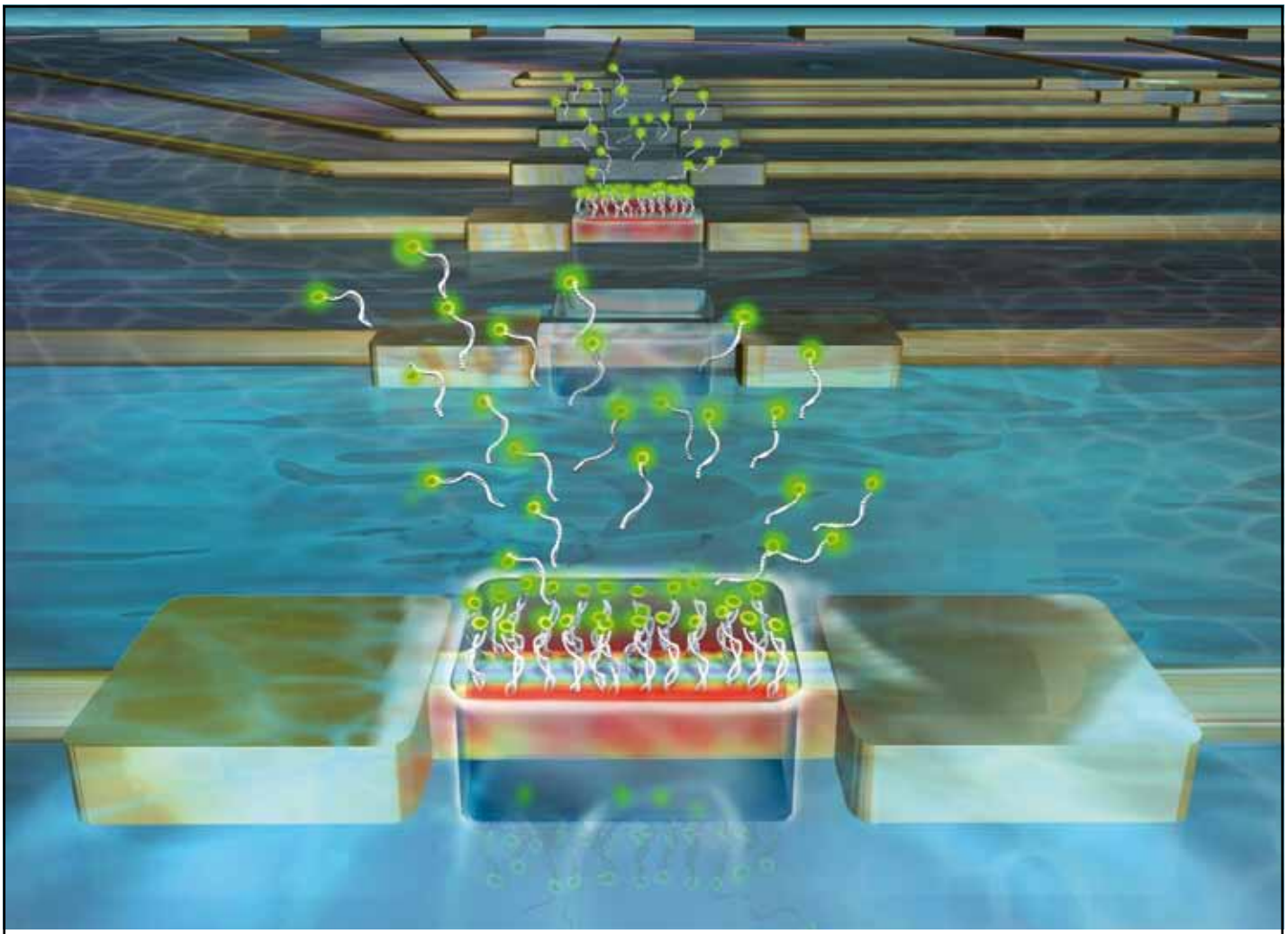

Featuring work from the group of Professor R. Bashir in the Department of Electrical and Computer Engineering, the Department of Bioengineering, and the Micro and Nanotechnology Laboratory (MNTL), University of Illinois at Urbana-Chapaign, Urbana, IL, USA.

Title: Localized heating on silicon field effect transistors: Device fabrication and temperature measurements in fluid.

A new dimension to present sensing systems is introduced by enabling dual purpose silicon transistor-heaters that serve both as field effect sensors and temperature controllers that could perform localized bio-chemical reactions.

As featured in:

See Bashir *et al., Lab Chip*, 2009, **9**, 2789–2795.

RSC Publishing

www.rsc.org

Registered Charity Number 207890

Localized heating on silicon field effect transistors: Device fabrication and temperature measurements in fluid

Oguz H. Elibol,†‡[ab] Bobby Reddy Jr.,†[df] Pradeep R. Nair,[ab] Brian Dorvel,[f] Felice Butler,[ac] Zahab S. Ahsan,[a] Donald E. Bergstrom,[ac] Muhammad A. Alam[ab] and Rashid Bashir†*[def]

Received 26th March 2009, Accepted 21st July 2009
First published as an Advance Article on the web 6th August 2009
DOI: 10.1039/b906048k

We demonstrate electrically addressable localized heating in fluid at the dielectric surface of silicon-on-insulator field-effect transistors *via* radio-frequency Joule heating of mobile ions in the Debye layer. Measurement of fluid temperatures in close vicinity to surfaces poses a challenge due to the localized nature of the temperature profile. To address this, we developed a localized thermometry technique based on the fluorescence decay rate of covalently attached fluorophores to extract the temperature within 2 nm of any oxide surface. We demonstrate precise spatial control of voltage dependent temperature profiles on the transistor surfaces. Our results introduce a new dimension to present sensing systems by enabling dual purpose silicon transistor-heaters that serve both as field effect sensors as well as temperature controllers that could perform localized bio-chemical reactions in Lab on Chip applications.

Introduction

The pervasive use of silicon field-effect transistors as switching elements in integrated circuits has revolutionized all aspects of modern life.[1–4] The field effect structures have also been used as chemical sensors for many years[5] and, more recently, their nanoscale manifestations have proven to be promising candidates for label-free high-sensitivity detection of biomolecules.[6,7] A critical function needed in integrated lab-on-chip devices is precise local control of temperature in fluid since generally all bio-chemical reactions are temperature driven. The rapid, localized, and precise heating of fluids in the range of microliters to as small as a few picoliters is important for a wide range of microfluidic applications. DNA amplification by polymerase chain reaction (PCR) is a prime example of such an application, where precise cycling of reagents between three temperatures in the range of 50–90 °C is performed.[8] Other applications include densely packed integrated sensors with distinct active surfaces,[9] localized temperature induced cell lysis,[10] investigation of reaction kinetics, biological studies, and organic/inorganic chemical synthesis. If both of these needs – that for label-free high sensitivity biomolecular sensors, and that for the precise control of temperature with high spatial resolution – could be combined into a single element, a new dimension of devices would be introduced, and such multi-functional transistors will find broad applications in many systems that had heretofore required separate components for each function.

Thus far, most efforts towards localized on-chip heating have focused on micro-fluidic systems with conduction-based heating *via* miniaturized Peltier elements,[11] integrated resistive heaters,[12,13] or Joule heating under electroosmotic flow.[14] These methods usually require a heated surface that is in close or direct contact with the fluid to be heated, as well as the heating of large substrate areas possibly preventing the integration of multiple analysis functions on a single substrate. An approach using a tungsten lamp as an IR source to rapidly heat small volumes of solution has been demonstrated,[15] but scaling up this technique remains challenging.

Microwave dielectric heating, on the other hand, fundamentally differs from conduction based heating due to its non-contact mode of delivering energy to the target fluid. In this case, microwave energy is delivered directly to the intended sample with no interference from the substrate.[16] Furthermore, the heating can be made to be more spatially selective by simply confining the electric fields to the desired regions in the microfluidic channel. Also, due to the lack of reliance on thermal diffusion in microwave heating, faster thermocycling rates and thus reduced reaction times can be achieved, compared to traditional techniques.[17] The total amount of power (P) converted into thermal energy with this method is given by $P = \omega\varepsilon_0\varepsilon''(\omega)|E|^2$ where ω is the applied frequency, $\varepsilon''(\omega)$ is the frequency-dependent loss of the local dielectric constant (encapsulates the relative response of the molecules to the applied field into one constant), and the local electric field E.[16] For high conductivity mediums, $\varepsilon''(\omega)$ can be represented as $\varepsilon''(\omega) = \varepsilon''_d(\omega) + \frac{\sigma}{\varepsilon_0\omega}$, where the first term is the energy dissipation

[a]*Birck Nanotechnology Center, Purdue University, West Lafayette, IN, 47907, USA*
[b]*School of Electrical and Computer Engineering, Purdue University, West Lafayette, IN, 47907, USA*
[c]*Department of Medicinal Chemistry and Molecular Pharmacology, Purdue University, West Lafayette, IN, 47907, USA*
[d]*Department of Electrical and Computer Engineering, University of Illinois at Urbana-Champaign, 208 North Wright Street, Urbana, IL, 61801, USA*
[e]*Department of Bioengineering, University of Illinois at Urbana-Champaign, 208 North Wright Street, Urbana, IL, 61801, USA*
[f]*2000 Micro and Nanotechnology Laboratory, MC-249, University of Illinois at Urbana-Champaign, 208 North Wright Street, Urbana, IL, 61801, USA. E-mail: rbashir@illinois.edu; Fax: (217) 244-6375; Tel: (217) 333-3097*
† Authors have contributed equally
‡ Now at Intel Corporation, Santa Clara, CA, USA.

due to dielectric relaxation, and the second term represents the conduction losses which can be approximated as the ratio of the conductivity of the buffer to the applied frequency.[18]

Several works have demonstrated the use of microwave heating for a variety of applications, including the heating of biological cells,[19] PCR,[20,21] and isolation of DNA.[22] In all of these cases, however, macroscale microwaves have been used, which will be difficult to scale down to microfluidic devices. On chip microwave heating has been demonstrated with miniaturized microwave elements with transmission lines,[23] as well as with thermocycling of PCR buffer solution in a microfluidic well using microwave energy.[24] In another approach, direct heating of the fluid is also possible through dielectric relaxation at microwave frequencies,[25] but the spatial temperature profile is dependent on the localization of the electric field, and requires wave guiding due to the relatively short wavelengths used.

In this work, we present the localized microwave heating of the fluid in the immediate vicinity of dual purpose sensor-heater field effect transistors. Local control of temperature on the gate dielectric of the transistors could also be achieved resistively by increasing the power dissipated through the active area. However, the relatively low doping levels of the silicon transistor active area mandates high electrical biases for heating, which results in dielectric breakdown near the drain-edge and subsequent current leakage through the breakdown spot to the fluid. Previous work has also demonstrated that the application of microwaves has the potential for much higher increases in temperature for a given power than resistive techniques.[26] Here, we demonstrate a novel heating approach by applying time-varying voltages[27] at radio frequencies for the Joule heating of the mobile ions responding to the electric field within the double layer at the surface of the dielectric layer. Since there is no direct current flow, the technique can be used with relatively high electrical resistance materials. Due to the mobile ions in the double layer, only the high conductivity region near the surface is heated, thus providing a method to precisely localize heating within a few nanometers of the insulator surface of the devices, with high spatial resolution due to the separate addressability of each device to be heated.

Materials and methods

Device fabrication

Fully CMOS compatible fabrication techniques were used to realize the silicon field effect devices. 8 inch bonded Silicon on Insulator (SOI) wafers (SOITEC), doped p type at 10^{15}/cm^2 with a buried oxide thickness of 1450 Å and superficial silicon layer thickness of 550 Å were laser cut into 4 inch wafers (Ultrasil Corp.) and used as a starting material. The top silicon was thinned down to 30 nm *via* dry oxidation performed at 1000 °C for 14 min. Subsequently, the top oxide layer was etched away using buffered oxide etch (BOE) for 30 sec. The active area was lithographically defined, and a hard mask for etching the silicon was formed by wet etching the remaining oxide. The exposed silicon was dry etched for 15 seconds using a STS Deep RIE machine (SF_6, 300 W, 100 mT, 30 sccm flow rate) to form the active areas. Next, the wafer was oxidized for 7 minutes at 1000 °C to form an implant slowdown layer of 200 Å. A photoresist implant mask defined by lithography was used to implant dopants. Source and drain areas were degenerately doped by implantation of Boron at 10 KeV at a dose of 10^{14} cm^{-2} and tilt of 7°. The implant mask was then stripped off and the dopant activation and gate oxidation growth, including sidewalls, were performed at 1000 °C for 5 min to grow a gate oxide of ~300 Å (Fig. 1a, part 1). Contacts to the active area were defined by lithography utilizing a liftoff process. Before metal evaporation, vias were formed on the silicon dioxide over the contact regions *via* etching for 25 sec using BOE. An adhesion layer of 200 Å of titanium followed by a 800 Å layer of platinum was evaporated to form metal contacts (Fig. 1a, part 2). After the liftoff process, Rapid Thermal Annealing (RTA) was performed at 500 °C for 180 sec in order to lower the contact resistance. Plasma Enhanced Chemical Vapor Deposited (PECVD) oxide was deposited as a metal passivation layer in order to minimize the parasitic conductance through the fluidic environment (Fig. 1a, part 3). The 5000 Å thick nitride rich PECVD layer was deposited using a STS 310 PECVD reactor, using nitrous oxide flow at 249 sccm, and 4% silane in argon flow at 1120 sccm. Deposition was performed at 300 °C, at 650 mT, using a plasma power of 20 W for 18 min. Oxide directly over the pad areas was

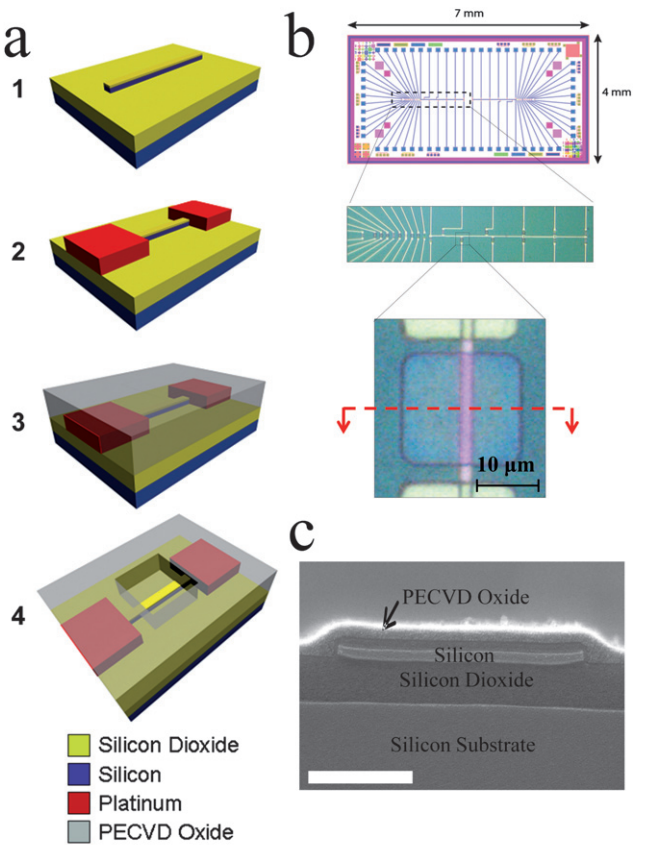

Fig. 1 Device fabrication and structure. a, Fabrication flow for the FET sensors. b, Top – schematic showing the device layout – the chip is 4 by 7 mm, with the contact pads at the periphery of the chip. Center – optical micrograph of a portion of the chip; devices can be independently addressed, with separate source/drain contacts or a common drain and separate sources. Bottom – optical micrograph of one device. c, SEM micrograph of a cross section through a device. Scale bar: 500 nm.

etched using BOE to expose the pads for probing. Next, areas over the active area of the devices were defined by lithography. The wafer was then diced into individual dies of size 4 mm by 7 mm (Fig. 1b). Individual dies were then dry etched using an isotropic RIE (90 W, CF_4, 18 mtorr, 15 mins). This step results in the final device structure as shown in Fig. 1a, part 4 (SEM cross section shown in Fig. 1c). Devices were designed to have an active area width of 2 μm and varying lengths of 5, 10 or 20 μm in length depending on the device location.

Fluorescent dye attachment

5(6)-Carboxy-X-rhodamine N-succinimidyl ester (ROX SE) was used for covalent attachment on device surfaces previously derivatized to expose an amine terminated surface. In short, surfaces were prepared as follows: After piranha cleaning, rinsing, and drying to expose surface hydroxyl groups, chips were placed in a sealed glass container containing a smaller vial filled with 5% (3-aminopropyl)dimethylethoxysilane in toluene, and were kept in a convection oven at 100 °C for 24 hours to form a vapor deposited monolayer. Chips were allowed to cool down to room temperature and were rinsed with 2-propanol, methanol, and DI water, and were dried under nitrogen flow. The dye was reacted with the surface by placing the chips in a solution of 200 μM of ROX SE in 150 mM of sodium phosphate buffer at pH 8.3 for 3 hours. Next, the chips were rinsed in 2-propanol, methanol, and DI water, and were dried under nitrogen.

Setup for application of heat and measurement of temperature

A Nikon Eclipse 600 fluorescence microscope was used to image the surface of the chips, using a TRITC filter to image the ROX dye. Images were captured with a high resolution cooled CCD camera (Penguin 600CL). Intensity quantification was extracted from captured images using MATLAB. All fluorescence images provided were performed in a wet ambient.

The chips were placed on a brass plate that functioned as a chuck to form the back contact. Micromanipulator probes were used to contact the appropriate pads on the chip. The source and drain contacts were shorted and an AC bias was applied between the source/drain and the back contact, as is shown in Fig. 2a, top. To obtain relatively high amplitude AC voltages, a RF power amplifier (EIN - Model 2100L - 50dB) was used in conjunction with a function generator (Agilent 33120A). Before heating the devices a droplet of buffer solution was dispensed to cover the devices without making contact to the contact electrodes or probe needles. A 10 MHz AC bias was applied for an appropriate time depending on the experiment. The devices were then configured with a standard DC scheme for sensing (a small voltage was applied between drain and source while measuring the current as shown in Fig. 2a, bottom), and transfer characteristics were extracted. The devices exhibit near ideal transfer characteristics (Fig. 2b) and remain operational in the voltage range used after heating with negligible increase in leakage current (Fig. 2b inset).

Localized temperature measurements

To find the decay constant as a function of temperature, experiments were performed on four different devices at four varying

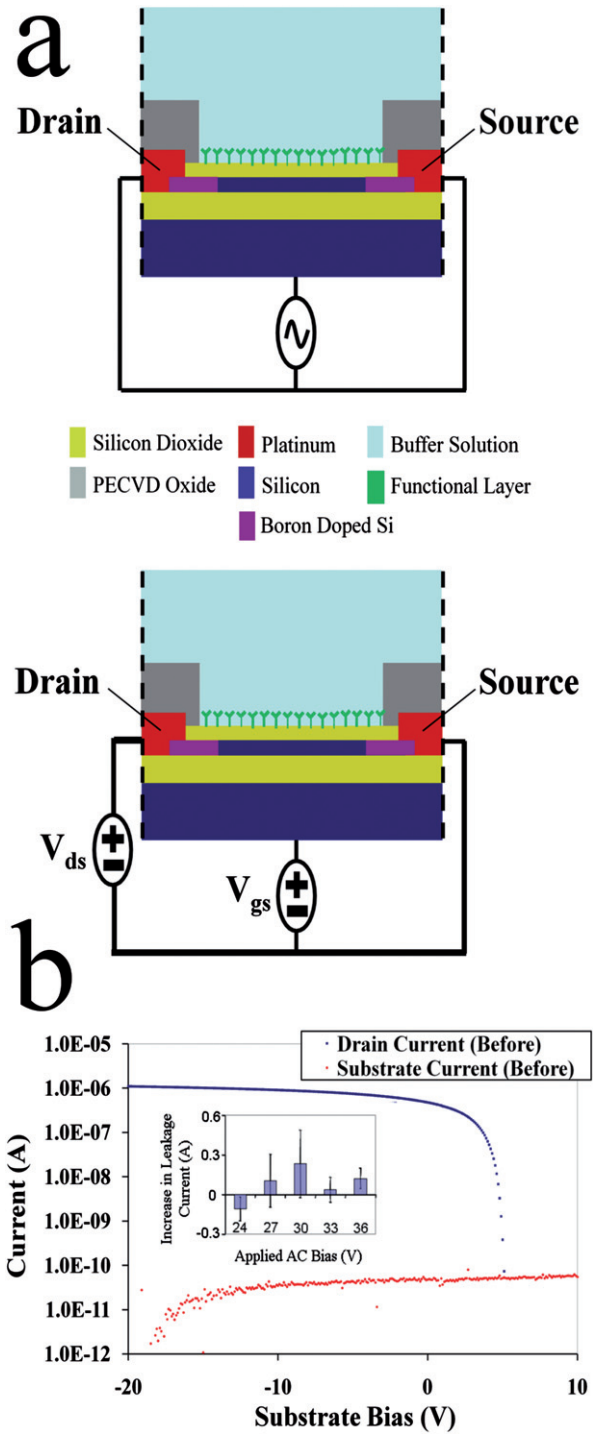

Fig. 2 AC heating scheme. a, Scheme for individual AC heating of the devices. b, Source–drain current for a device after heating. Inset: No significant increase in leakage current was observed after various applied AC heating biases.

temperature points. In all experiments, the incident intensity was kept constant. The fluorescence images of devices at known temperatures were acquired at regular intervals of 15 seconds for a total time of 5 min. Device intensities were plotted as a function of time, and the rate constant was extracted. The extracted rate constants were plotted as a function of temperature. Data was

interpreted and fitted to curves assuming that the rate constant is related to the temperature through an Arrhenius equation. Generation of the temperature maps was performed by fitting the intensity of each pixel in the series of acquired images using the same procedure, and assigning the temperature to each pixel as a result of the performed fit.

Results and discussion

Using the method described above, we demonstrate the ultra-localized dielectric heating of fluids using silicon-on-insulator field-effect devices fabricated with CMOS compatible techniques. The process used to fabricate these devices is compatible with high volume and low cost fabrication with the potential for integration with other miniaturized components on the same platform (Fig. 1b). Each device can be addressed through two electrical contacts on either side, and operated as a field effect sensor.[28] Electrically addressable heating is accomplished by applying an alternating voltage at a frequency of 10 MHz between the active area and the substrate, which are separated by an electrically insulating **b**uried silicon di**ox**ide (BOX) dielectric layer[26] (Fig. 2a).

Selection of a fluorophore for nanoscale thermometry

Before specific applications are demonstrated using the 'transistor-heater' hybrids, we need to demonstrate the effectiveness of localized heating and calibrate the temperature close to the surface. Fluorescent molecule probes have been used in microfluidic systems for monitoring increase in temperature of *bulk* fluid volumes by measuring the decrease in fluorescence due to change in quantum efficiency of the fluorophores.[29,30] This classical technique is inappropriate for our application given the localized nature of the temperature profile and the additional noise introduced by background fluorescence in the fluid. Instead, we use a variation of the 'bulk' fluorescence technique to measure temperature close to the surface in fluid. Specifically, instead of using the fluorescent decay of quantum efficiency as a marker of temperature, we chose the fluorescent molecule Rhodamine X whose degree of photobleaching depends on temperature (Arrhenius activation) and is proportional to incident light intensity, *i.e.* $I = Ae^{-k(T)t} + I_{bg}$, where A is the initial net intensity (without the background), and I_{bg} the background fluorescence intensity.[31] Rhodamine X contains the Rhodamine 101 chromophore, whose quantum efficiency is almost 1.0 and is known to be nearly independent of changes in temperature[32] (Fig. 6a).

Fluorescence interference contrast issues on FET sensors

Fluorescence interference contrast (FLIC) is a phenomenon that has been discussed earlier,[33,34] though not examined on SOI substrates or on the gate oxide of transistors. When fluorescent molecules are placed in close vicinity to reflective surfaces, the emitted light propagates at an angle towards the reflective surface, is reflected back, and can either constructively or destructively interfere with the original light. The observed fluorescence signal is thus modulated based on the distance of the fluorophores from the reflective surface. In the course of this work, initial attempts were made to observe fluorescence from molecules that were immobilized directly on the thermal oxide on top of the active area of the devices (gate oxide $\sim$ 330 Å), but little to no fluorescence was observed. We examined this problem by studying the reflectance properties of molecules on oxides of different thicknesses. The thermal oxide/PECVD oxide stack over the active area of the devices (Fig. 3a) was varied from around 350 Å to 750 Å by employing a range of dry release times in the final fabrication step. All the chips were then immobilized with the ROX dyes used for the temperature measurement studies. Results are shown in Fig. 3b and 3c. The fluorescence signal can be seen to depend dramatically on the thickness of the oxide upon which the molecules are immobilized, both over the active area and in the etchback window. For all fluorescent studies and temperature measurements in this work, a gate oxide thickness of around 750 Å was used, precisely due to these observed results. It should be noted that when the devices are to be used for sensing, a thinner gate oxide would be used since the maximum sensitivity for field effect sensors is achieved when the molecules to be detected are as close to the gate oxide as possible. We used a gate oxide thickness of 750 Å only to demonstrate the localized heating method since we use fluorescence as the means to measure the temperatures at the device surface.

Measurement of temperature at the surface of the sensors

Once the device design and fabrication was completed and the fluorescent dye was covalently attached to the surface, we heated

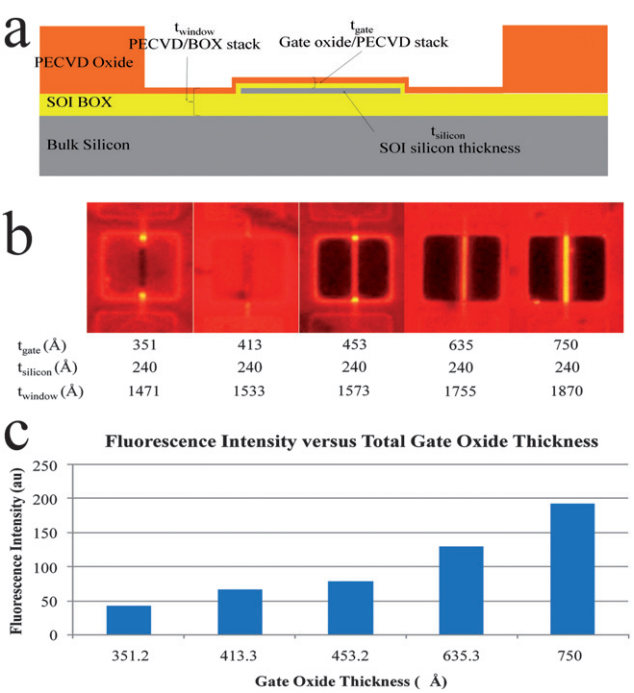

Fig. 3 FLIC phenomena on transistor surfaces. a, Cross section of the devices through the red line in Fig. 1b, bottom. t_{gate} is the gate oxide thickness and t_{window} is the total thickness of the remaining PECVD oxide/buried oxide stack. b, Fluorescence pictures and corresponding oxide and silicon thicknesses for a spectrum of depth profiles. The FLIC phenomena can be clearly observed, and fluorescence intensities vanish as t_{gate} approaches the thickness of the thermal oxide. c, Bar graph quantifying the fluorescence intensities from b.

the transistors *via* RF dielectric heating. The position-resolved decay in fluorescence, and hence the pixel-specific temperature increase indicated non-uniform heating across the device. The temperature of the distinct regions was determined by grouping and averaging the fluorescence intensity over the regions of interest. The data obtained by averaging the fluorescence intensity as a function of time was fitted to the function in the form above at two different voltages (Fig. 4). Our results show

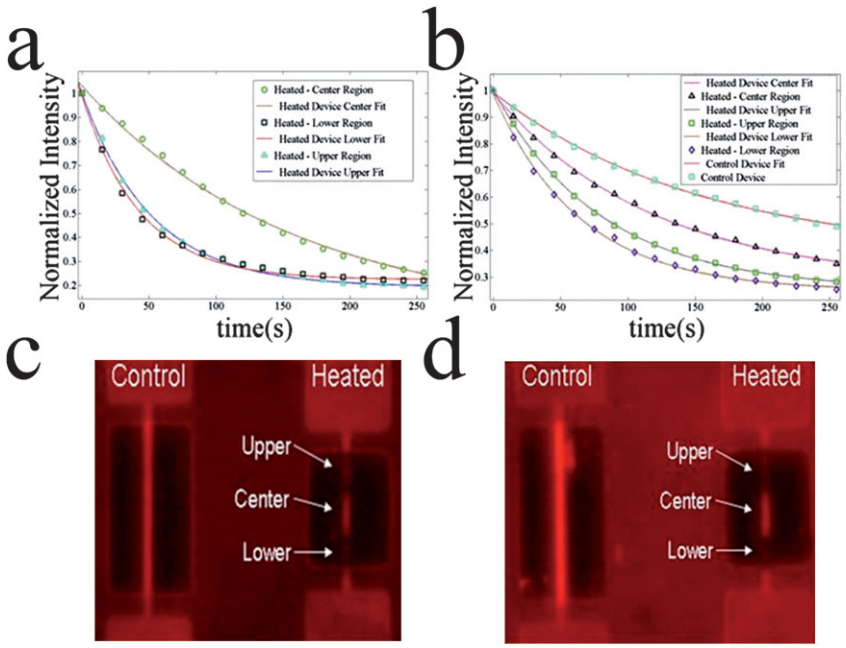

Fig. 4 Demonstration of the enhanced photobleaching at elevated temperatures. a, b, Sample photobleaching decay curves acquired during the application of 27 V_{rms} and 33 V_{rms}, respectively. In b, the decay curve for a control device is also plotted for comparison – the enhanced photobleaching decay due to the increase in temperature is evident. c, d, The corresponding fluorescent images are shown to the right taken at 3 min exposure, including a control device.

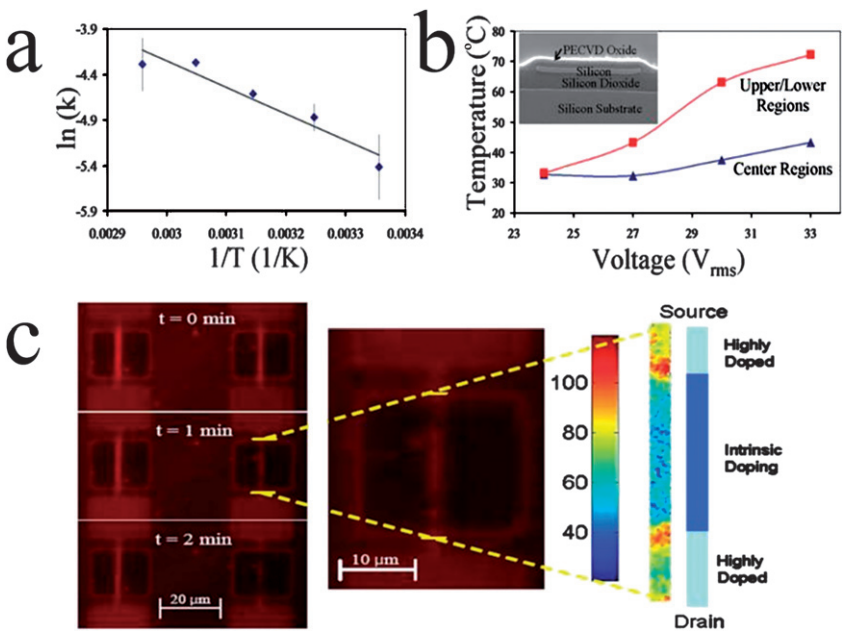

Fig. 5 Demonstration of the nanoscale thermometry method. a, Calibration curve to correlate the temperature with the decay constant. b, The extracted temperature *versus* voltage curve demonstrating the effect of the AC bias on temperature. The temperature increases are seen to be much higher for the upper and lower regions of the device for a given applied AC voltage. Inset: a SEM cross section of a typical device used for these measurements. c, The heating spatial profile for the devices. On the left, a typical bleaching experiment is shown. The decay rate for the top and bottom regions of the device (the doped regions) is clearly faster than that for the center regions (undoped regions). The center image is a sample picture from which the plots on the right were generated.

that the lower and upper portions, corresponding to regions which are heavily p-type doped (>10^{19}) to form a proper contact to the undoped region at the center of the device reach a higher temperature than the middle of the device. It is also evident that increasing the applied voltage results in an increase in the rate of fluorescence decay, translating into a higher temperature. We obtain the constants A, k, and I_{bg} in the equation mentioned previously through a separate calibration experiment, where the structure is uniformly heated at a given temperature by an external heater and the decay of the fluorescent signal is recorded. Given the constants, we use the position-resolved intensity of each pixel during actual operation of the device to infer back the temperature and generate a calibration curve (Fig. 5a). Using this calibration data, we obtained the temperature on the surface of the devices as a function of the applied voltage, finding that a range of 33–75 °C is obtainable with an AC voltage range of 24–33 V_{rms} using a device 10 μm in length (Fig. 5b). This method was further extended for the temperature mapping over the regions of interest by performing the curve fit for every pixel of the images obtained. By relating the decay constant to the temperature for each pixel, the surface temperature as a function of location can be obtained (Fig. 5c). The heat map shows that the increase in the temperature is non-uniform and there is an increase in the temperature at the edges of the device as a result of field crowding due to geometric effects and due to a transition from a highly doped to a lightly doped region. Hence, sharp temperature gradients can be created simply through the control of the doping profile of such devices. It should be noted that the exact temperature profile depends on the counter-ion profile on the surface and will vary as a function of the molecules on the surface, and our experiments serve as a benchmark for the approximate temperatures that can be obtained using the method.

We also performed additional control experiments to validate the proposed heating mechanism and measurement technique. First, we experimentally showed that the fluorophore used, ROX, emits fluorescence intensities that are independent of temperature (Fig. 6a), which demonstrates that measured decreases in fluorescence are due to bleaching, instead of modulation of quantum efficiency. Also, to further investigate the photobleaching measurement of temperature, experiments were performed in a very similar fashion to the actual temperature measurement, but without exposing the devices to UV light. When the AC voltage was applied to heat the devices without light excitation (Fig. 6b, top), no enhanced decay of the fluorescence was observed. Further, when both the voltage and light excitation were applied, but in a dry state without the surrounding fluid and hence no mobile ions, again no enhanced decay was observed (Fig. 6b, middle). However, when light, AC voltage, and fluid were applied (Fig. 6b, bottom), normal enhanced decay results were achieved. The fact that enhanced decay is observed only when all three conditions are applied proves that the enhanced fluorescence bleaching is due to dielectric heating of the fluid, as opposed to other possible theories that may have yielded the same results – such as electric field mediated removal of the molecules *via* redox potentials, or instability of the fluorophores due to increased temperatures.

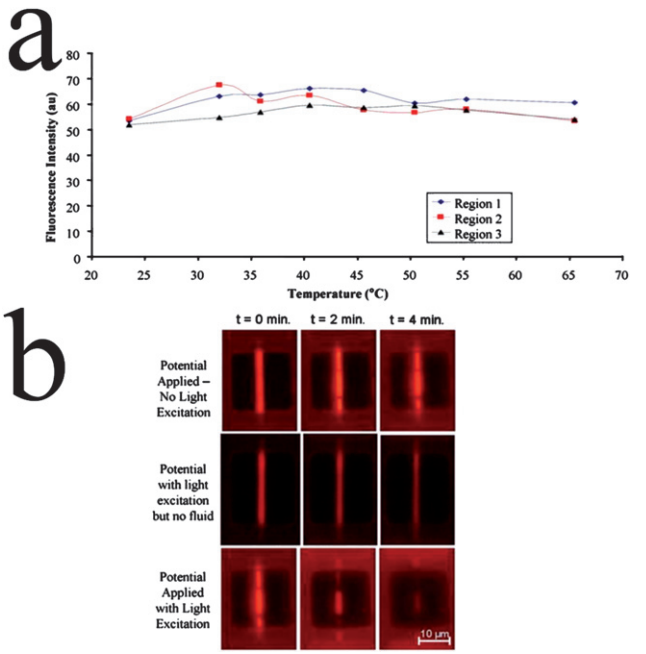

Fig. 6 Control experiments for the heating and temperature measurement. a, Plot showing the independence of fluorescence intensity of the immobilized ROX molecules used for photobleaching measurements on temperature. For all 3 regions of the device (upper, middle, lower) no dependence of the quantum efficiency of the fluorophores on temperature is observed. b, Control experiment to lend additional evidence to the proposed phenomena underlying the photo-bleaching temperature measurements and the heating mechanism. In the upper set of pictures, the device is heated without continuous light excitation (devices were exposed only briefly to light to capture the pictures), and hence without photo-bleaching. In the middle set of pictures, an AC voltage is applied to the device but without any fluid. In the bottom set of pictures, when light and AC voltage is applied to the devices in fluid, enhanced decay of the fluorescence is observed.

Conclusion

Our results demonstrate the integration of an additional dimension to standard transistor sensing elements. This can be a powerful tool for lab-on-a-chip applications, enabling the precise spatial and temporal control of temperature profiles on chip simultaneous with biomolecular sensing. The surface fluorescence thermometry technique can be widely utilized in applications requiring the study of temperature profiles in nanoscale structures and interfacial heat transfer studies. These field effect sensor-heater hybrids could be used to develop a variety of new tools for lap-on-a-chip applications, including localized biochemical reactors, highly integrated PCR systems, and localized heat mediated cell manipulators while also enabling ultra-sensitive, label-free detection of desired analytes.

Acknowledgements

We acknowledge the use of Micro and Nanotechnology Laboratory at UIUC and the Birck Nanotechnology Center at Purdue for device fabrication, and UIC NCF staff for assistance with PECVD deposition. We are grateful to T. Sands (Purdue), D. Peroulis (Purdue), D. Cahill (UIUC), and W. P. King (UIUC)

for helpful suggestions and discussions. This work was initially funded by NIH (R21-EB006308), NSF (ECS 0554990), a seed grant from the Indiana Elks administered through the Purdue University Cancer Center, and now by NIH (R01CA20003).

References

1 J. S. Kilby, Miniaturized electronic circuits, U.S. patent 3,138,743 (1964).
2 D. H. Kim, J. H. Ahn, W. M. Choi, H. S. Kim, T. H. Kim, J. Z. Song, Y. G. Y. Huang, Z. J. Liu, C. Lu and J. A. Rogers, Stretchable and foldable silicon integrated circuits, *Science*, 2008, **320**, 507–511.
3 R. R. Schaller, Moore's Law: Past, Present, and Future, *IEEE Spectrum*, 1997, **34**, 52–59.
4 W. S. Bacon, The Transistor's 20th Anniversary: How Germanium and a Bit of Wire Changed the World, *Popular Science*, 1968, **192**, 80–84.
5 P. Bergveld, Thirty years of ISFETOLOGY what happened in the past 30 years and what may happen in the next 30 years, *Sens. Actuators, B*, 2003, **88**, 1–20.
6 E. Stern, J. F. Klemic, D. A. Routenberg, P. N. Wyrembak, D. B. Turner-Evans, A. D. Hamilton, A. A. LaVan, T. M. Fahmy and M. A. Reed, Label-free immunodetection with CMOS-compatible semiconducting nanowires, *Nature*, 2007, **445**, 519–522.
7 Y. Cui, Q. Wei, H. Park and C. M. Lieber, Nanowire nanosensors for highly sensitive and selective detection of biological and chemical species, *Science*, 2001, **293**, 1289–1292.
8 M. U. Kopp, A. J. De Mello and A. Manz, Chemical Amplification: continuous-flow PCR on a chip, *Science*, 1998, **280**, 1046–1048.
9 D. L. Huber, R. P. Manginell, M. A. Samara, B. Kim and B. C. Bunker, Programmed adsorption and release of proteins in a microfluidic device, *Science*, 2003, **301**, 352–354.
10 L. C. Walters, S. C. Jacobson, N. Kroutchinina, J. Khandurina, R. S. Foote and J. M. Ramsey, Microchip device for cell lysis, multiplex PCR amplification, and electrophoretic sizing, *Anal. Chem.*, 1998, **70**, 158–162.
11 G. Maltezos, M. Johnston and A. Scherer, Thermal management in microfluidics using micro-Peltier junctions, *Appl. Phys. Lett.*, 2005, **87**, 154105.
12 I. Park, Z. Li, A. P. Pisano and R. S. Williams, Selective surface functionalization of silicon nanowires *via* nanoscale Joule heating, *Nano Lett.*, 2007, **7**, 3106–3111.
13 C. Y. Lee, G. B. Lee, J. L. Lin, F. C. Huang and C. S. Liao, Integrated microfluidic systems for cell lysis, mixing/pumping and DNA amplification, *J. Micromech. Microeng.*, 2005, **15**, 1215–1223.
14 P. Liu, T. S. Seo, N. Beyor, K. J. Shin, J. R. Scherer and R. A. Mathies, Integrated portable polymerase chain reaction-capillary electrophoresis microsystem for rapid forensic short tandem repeat typing, *Anal. Chem.*, 2007, **79**, 1881–1889.
15 B. C. Giordano, J. Ferrance, S. Swedberg, A. F. R. Huhmer and J. P. Landers, Polymerase chain reaction in polymeric microchips: DNA amplification in less than 240 seconds, *Anal. Biochem.*, 2001, **291**, 124–132.
16 N. E. Bengtsson and T. Ohlsson, Microwave heating in the food industry, *Proc. IEEE*, 1974, **62**, 44–45.
17 Y. V. Bykov, K. I. Rybakov and V. E. Semenov, High-temperature microwave processing of materials, *J. Phys. D: Appl. Phys.*, 2001, **34**, R55–75.
18 C. Gabriel, S. Gabriel, E. H. Grant, B. S. J. Halstead and D. M. P. Mingos, Dielectric parameters relevant to microwave dielectric heating, *Chem. Soc. Rev.*, 1998, **27**, 213–223.
19 Y. Nikawa, K. Yamamoto, S. Izumidate and N. Kubota, An Irradiation System of Pulsed Modulation Microwaves to Culture Cells, 18th International Conference IEEE Engineering Medical Biological Society, 1996, **5**, pp.1865–1866.
20 C. Fermer, P. Nilsson and M. Larhed, Microwave-assisted high-speed PCR, *Eur. J. Pharm. Sci.*, 2003, **18**, 129–132.
21 P. A. Auroux, J. J. Shah, J. Booth, M. V. Rao, L. E. Locascio and M. Gaitan, Microfluidic method for thermal cycling by microwave dielectric heating, Proceedings Micro Total Analysis Systems, 2006, **2**, pp. 1465–1467.
22 D. C. Goodwin and S. B. Lee, Microwave miniprep of total genomic DNA from fungi, plants, protists and animals for PCR., *Biotechniques*, 1993, **15**, 438.
23 S. G. Sundaresan, B. J. Polk, D. R. Reyes, M. V. Rao and M. Gaitan, Temperature control of microfluidic systems by microwave heating, Proceedings of Micro Total Analysis Systems, 2005, **1**, pp. 657–659.
24 A. Sklavounos, D. J. Marchiarullo, S. L. R. Barker, J. P. Landers and N. S. Barker, Efficient miniaturized systems for microwave heating on microdevices, Proceedings Micro Total Analysis Systems, 2006, **2**, pp. 1238–1240.
25 J. J. Shah, S. G. Sundaresan, J. Geist, D. R. Reyes, J. C. Booth, M. V. Rao and M. Gaitan, Microwave dielectric heating of fluids in an integrated microfluidic device, *J. Micromech. Microeng.*, 2007, **17**, 2224–2230.
26 O. H. Elibol, B. Reddy Jr. and R. Bashir, Localized heating and thermal characterization of high electrical resistivity silicon-on-insulator sensors using nematic liquid crystals, *Appl. Phys. Lett.*, 2008, **93**, 131908.
27 A. J. De Mello, M. Habgood, N. L. Lancaster, T. Welton and R. C. R. Wootton, Precise temperature control in microfluidic devices using Joule heating of ionic liquids, *Lab Chip*, 2004, **4**, 417–419.
28 O. H. Elibol, B. Reddy Jr. and R. Bashir, Nanoscale thickness double-gated field effect silicon sensors for sensitive pH detection in fluid, *Appl. Phys. Lett.*, 2008, **92**, 193904.
29 J. Lou, T. M. Finegan, P. Mohsen, T. A. Hatton and P. E. Laibinis, Fluorescence-based thermometry: principles and applications, *Rev. Anal. Chem.*, 1999, **18**, 235–284.
30 D. Ross, M. Gaitan and L. E. Locascio, Temperature measurements in microfluidic systems using a temperature-dependent fluorescent dye, *Anal. Chem.*, 2001, **73**, 4117–4123.
31 L. Gui and C. L. Ren, Temperature measurement in a microfludic chips using photobleaching of a fluorescent thin film, *Appl. Phys. Lett.*, 2008, **92**, 024102.
32 T. Karstens and K. Kobs, Rhodamine B and Rhodamine 101 as Reference Substances for Fluorescence Quantum Yield Measurements, *J. Phys. Chem.*, 1980, **84**, 1871–1872.
33 A. Lambacher and P. Fromherz, Fluorescence interference-contrast microscopy on oxidized silicon using a monomolecular dye layer, *Appl. Phys. A: Mater. Sci. Process.*, 1996, **63**, 207–216.
34 C. M. Ajo-Franklin, C. Yoshina-Ishii and S. G. Boxer, Probing the Structure of Supported Membranes and Tethered Oligonucleotides by Fluorescence Interference Contrast Microscopy, *Langmuir*, 2005, **21**(11), 4976–4983.